

ORIGINAL ARTICLE

NaNbO₃-BaTiO₃-NaSbO₃ lead and potassium-free ceramics with thermally stable small-signal piezoelectric propertiesHe Qi¹ | Haibo Zhang² | Ruzhong Zuo¹ ¹Institute of Electro Ceramics & Devices, School of Materials Science and Engineering, Hefei University of Technology, Hefei, China²College of Materials Science and Engineering, State Key Laboratory of Material Processing and Die and Mould Technology, Huazhong University of Science and Technology, Wuhan, China**Correspondence**Ruzhong Zuo, Institute of Electro Ceramics & Devices, School of Materials Science and Engineering, Hefei University of Technology, Hefei, China.
Email: rzuo@hotmail.com**Funding information**

The joint fund of National Natural Science Fund Committee and Large Devices of Chinese Academy of Science, Grant/Award Number: U1432113; National Natural Science Foundation of China, Grant/Award Number: 51332002

Abstract

A new lead-potassium-free ceramic of (0.9-*x*)NaNbO₃-0.1BaTiO₃-*x*NaSbO₃ (NN-BT-*x*NS) was successfully prepared via a solid-state reaction method. The microstructure, phase structure, dielectric, ferroelectric, and piezoelectric properties were investigated as a function of NS content. The substitution of NS for NN was found to dramatically change the grain morphology from cube-like grains typical for alkaline niobate-based ceramics to conventional sphere-like grains especially for Pb-based perovskite ceramics. A normal to relaxor ferroelectric phase transformation was accompanied by a tetragonal (*T*) to rhombohedral (*R*) phase transition. A composition-temperature phase diagram demonstrated a vertical morphotropic phase boundary between *T* and *R* phases in the composition range of *x*=0.03-0.04, where optimum electrical properties of *d*₃₃=252 pC/N, *k*_p=36%, *Q*_m=168, $\epsilon_{33}^T/\epsilon_0=2063$, and *T*_c=109°C were obtained in the *x*=0.035 ceramic sintered at 1260°C. Particularly, excellent temperature insensitivity of small-signal piezoelectric properties suggested large application potentials in various actuators and sensors in comparison with other typical lead-free materials.

KEYWORDS

ferroelectricity/ferroelectric materials, lead-free ceramics, morphotropic phase boundary, piezoelectric materials/properties

1 | INTRODUCTION

Lead-free piezoelectric ceramics have been extensively investigated in the past 10 years¹⁻¹⁰ for the purpose to replace conventional lead-based perovskite piezoelectric materials such as Pb(Zr,Ti)O₃, Pb(Mg_{1/3}Nb_{2/3})O₃, and so on. The relevant research work has become of great significance and urgency, considering big risks that the lead pollution might bring to human beings.

Typical lead-free material systems so far mainly include (Na,K)NbO₃ (NKN)-based solid solutions,^{1,6,7,11} modified BaTiO₃ (BT)-^{8,9,12} and (Bi_{0.5}Na_{0.5})TiO₃ (BNT)-based solid solutions.^{10,13-15} Piezoelectric and electromechanical properties of these materials have been significantly improved in the past few years by designing compositions lying in the proximity of two-ferroelectric phase boundaries. The

flattening of free energy profile for polarization switching by coexisting ferroelectric phases with different crystal symmetries provided a solid structural fundament for enhancing piezoelectric activities.^{8,16} As known, for industrial application of piezoelectric devices, not only the magnitude of piezoelectric properties but also their reliability such as temperature stability are equally important. BNT-based compositions exhibited temperature-stable medium piezoelectric properties owing to the existence of morphotropic phase boundary (MPB) between rhombohedral (*R*) and tetragonal (*T*) phases,¹³ yet the temperature range of the stability was strictly limited within <100°C by a high-temperature relaxor phase.^{10,17} High-performance BT- or NKN-based lead-free systems achieved significantly enhanced piezoelectric coefficient *d*₃₃ through largely sacrificing their Curie temperatures (*T*_c). Moreover, the

dependence of piezoelectric activities on the polymorphic phase transition or the polymorphic phase coexistence was believed to be responsible for high-temperature sensitivity of electrical properties for these two lead-free material systems,^{12,18–22} even though high-field piezoelectric coefficients were reported to exhibit a good temperature stability.^{23,24} Apart from this, the processing property of the ceramic powder and composition is also a key issue for mass production, such as tape casting for preparing ceramic tapes. The processing sensitivity seemed to exist in NKN-based lead-free compositions owing to the existence of highly hygroscopic potassium carbonates and the high volatility of K_2O at high temperatures.^{25,26} Particularly, typical cube-like grain morphology of NKN-based compositions would possibly make the sintering body less compacted and the ceramic film less smooth.

A lead- and potassium-free NN-based piezoelectric ceramic was reported as a potential candidate to address the above-mentioned issues. An orthorhombic (O) antiferroelectric NN at room temperature (RT) could transform into a T ferroelectric phase by adding $LiNbO_3$, $(Bi_{0.5}K_{0.5})TiO_3$ and BT.^{27–29} A phase-boundary composition in the proximity of a vertical R-T MPB was obtained by substituting BT and $CaZrO_3$ (CZ) for NN, achieving temperature-insensitive piezoelectric properties.³⁰ Nevertheless, in addition to insufficient piezoelectric properties, the cube-like grain morphology was still maintained, as compared with NKN-based lead-free ceramics. The poor piezoelectricity of NN-based ceramics might be mainly related to the strong ionic characteristics. In this work, another ABO_3 -type $NaSbO_3$ (NS) was used as a modifier of the phase structure, considering that the higher electronegativity of Sb^{5+} would make the NN-based perovskite more covalent. The addition of Sb^{5+} was believed to play a crucial role in the enhancement of piezoelectric properties of previously reported NKN-based ceramics.^{1,4,19,31} The microstructure, crystal structure, domain morphology, and various electrical properties were investigated as a function of NS content.

2 | EXPERIMENTAL PROCEDURE

The $(0.9-x)NN-0.1BT-xNS$ (NN-BT- xNS) ceramics were prepared by a solid-state reaction method using analytical-grade metal oxides and carbonates as raw materials. The powders were mixed thoroughly in ethanol using zirconia balls for 12 hour according to their compositional formula. The powder mixture was ball-milled again for 24 hour after calcination at $1000^\circ C$ for 5 hour, and then pressed into disk samples with a diameter of 10 mm under 100 MPa using polyvinyl alcohol (PVA) as a binder. The disk samples were sintered at $1220-1300^\circ C$ for 2 hour in air after burning out the binder at $550^\circ C$ for 4 hour. Silver

electrodes were fired on both sides of the samples at $550^\circ C$ for 30 minutes. The samples were poled under a dc field of 4 kV/mm for 30 minutes at RT in a stirred silicone oil bath.

The microstructure of the sintered samples was observed using a field emission scanning electron microscope (FE-SEM; SU8020, JEOL, Tokyo, Japan). Before the SEM observation, some samples were carefully polished and then thermally etched at $1000^\circ C$ for 30 minutes. The crystal structure at RT was analyzed by a powder X-ray diffractometer (XRD, D/MAX-RB, Rigaku, Tokyo, Japan) using a $Cu K\alpha$ radiation ($\lambda=1.5406 \text{ \AA}$). Dielectric properties as a function of temperature and frequency were measured by an LCR meter (Agilent E4980A, Santa Clara, CA). The quasi-static piezoelectric constant d_{33} was measured by a Belincourt meter (YE2730A, Sinocera, Yangzhou, China). The planar electromechanical coupling factor k_p and mechanical quality factor Q_m were determined by a resonance-antiresonance method with an impedance analyzer (PV70A, Beijing Band ERA Co., Ltd. China). The polarization versus electric field ($P-E$) and strain versus electric field ($S-E$) loops were measured using a ferroelectric test system (Precision multiferroelectric; Radiant Technologies Inc, Albuquerque, New Mexico) connected with an accessory laser interferometer vibrometer (AE SP-S 120E, SIOS Mebtechnils, GmbH, Ilmenau, Germany). The temperature-dependent d_{33} and k_p were measured at RT after poled samples were annealed at each different temperature during heating. The domain morphology observation was performed on a field emission transmission electron microscope (FE-TEM, JEM-2100F, JEOL, Japan) operated at 200 kV. For TEM examination, samples were first mechanically polished to a thickness of $\sim 20 \mu m$ and then ion-milled on a Precision Ion Polishing System (PIPS, Model 691, Gatan Inc., Pleasanton, CA, USA) at 5 kV. All specimens were annealed at $80^\circ C$ for at least 1 day to release the mechanical stress before the observation.

3 | RESULTS AND DISCUSSION

3.1 | Evolution of microstructure and phase structure

Figure 1 shows the grain morphology of NN-BT- xNS ceramics sintered at their optimum temperatures. All samples exhibited dense microstructure with a relative density of over 96%. Moreover, the grain size did not change obviously with changing the NS content (average grain size is $\sim 2.5 \mu m$), as estimated by a linear intersection method on polished surfaces (Figure 1E-H). It is worthy of note that the substitution of NS for NN significantly changed the grain morphology from cube-like grains for $x \leq 0.02$ to sphere-like grains for $x \geq 0.035$. The former is one of the

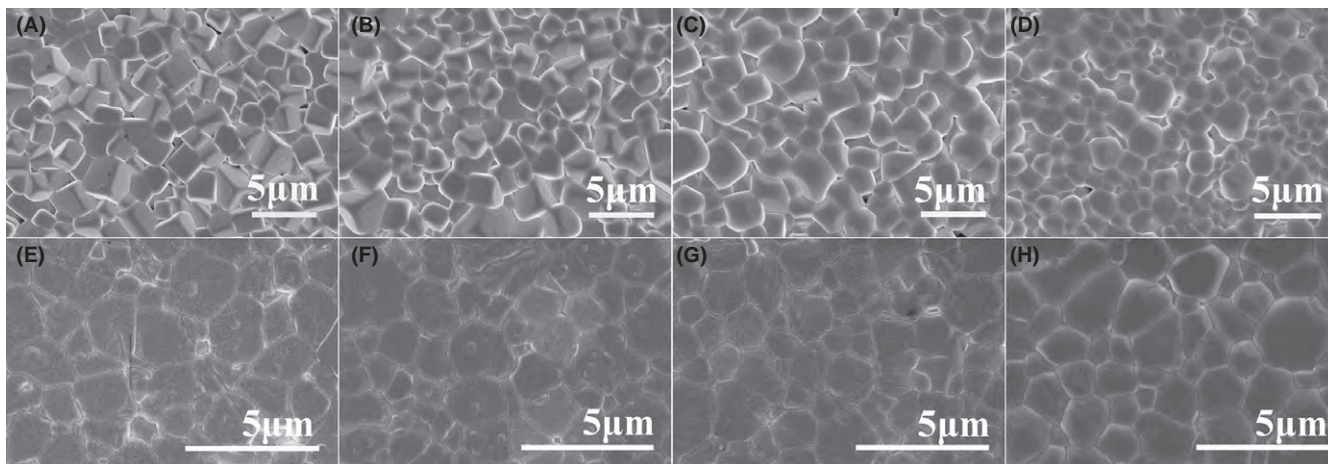


FIGURE 1 SEM micrographs on fractured surfaces of NN-BT- x NS ceramics with (A) $x=0$, (B) $x=0.02$, (C) $x=0.035$, and (D) $x=0.055$, and on polished and thermally etched surfaces of NN-BT- x NS ceramics with (E) $x=0$, (F) $x=0.02$, (G) $x=0.035$, and (H) $x=0.055$

typical features for alkaline niobate ceramics such as NKN-based lead-free ceramics, but the latter is a common morphology for nearly all Pb-based perovskite piezoelectric ceramics. The difference in grain morphology might have an effect on the compact density of the sintered samples and the tape casting process of the ceramic films.^{32–34} The irregularity of polyhedral particles tends to hinder particle mobility and their ability to attain dense packing configurations,³² further influencing the following densification process in combination with lower contact areas of two particles.³³ As Qin et al. reported,³⁴ slurries with particle morphologies of lower Hausdroff dimensionality have a higher viscosity for a given solid fraction. Compared with spherical particles, irregular polyhedral particles were

predicted to have a relatively small Hausdroff dimensionality value,³⁴ leading to unexpectedly increased slurry viscosity. Moreover, the elemental distribution of the sintered ceramics was analyzed using the $x=0.035$ composition as an example, as shown in Figure 2. It can be seen that all elements were homogeneously distributed in the ceramic, suggesting that a homogenous solid solution of NN-BT-NS was formed.

Figure 3A shows XRD patterns of NN-BT- x NS ceramics at RT. All diffraction peaks could be well indexed to a single perovskite structure, indicating the formation of single solid solutions in the investigated composition range. This should be related to the similar radius and charge valence of Nb⁵⁺ (0.64 Å, CN=6) and Sb⁵⁺ (0.61 Å,

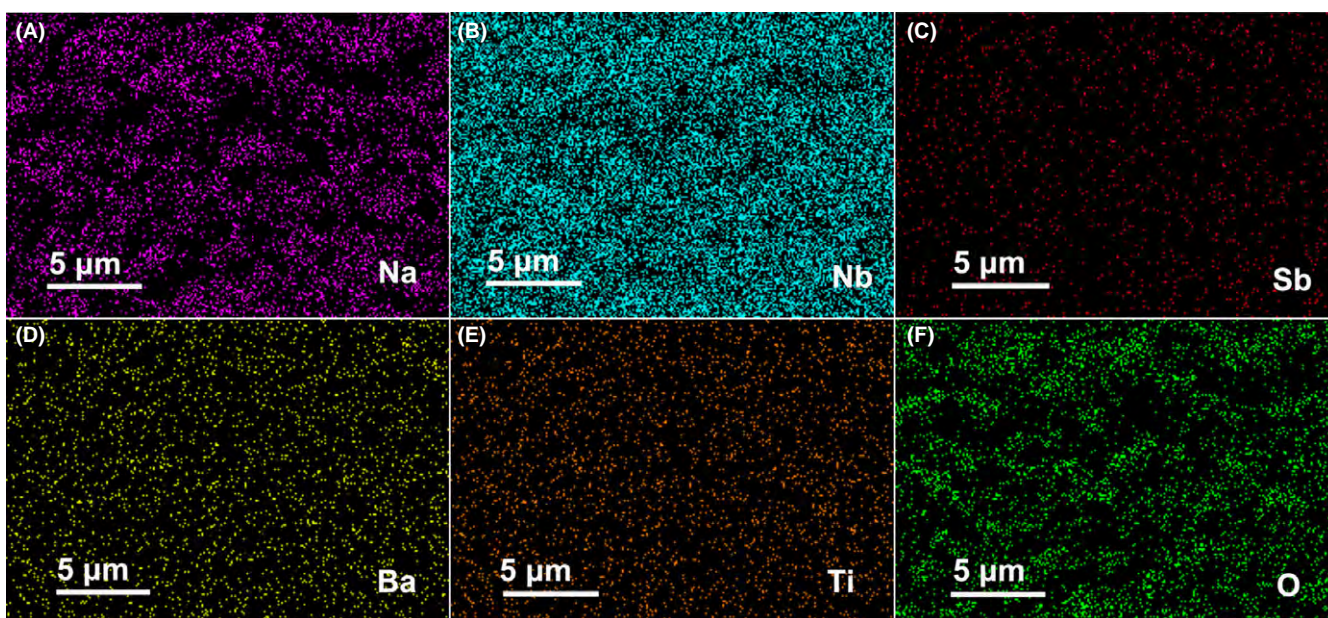


FIGURE 2 Element mapping on the polished cross-section of the $x=0.035$ sample [Color figure can be viewed at wileyonlinelibrary.com]

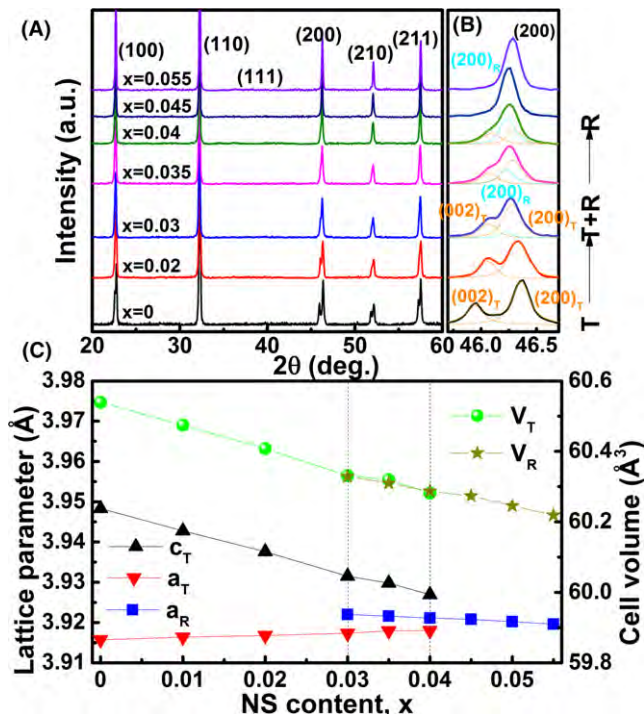


FIGURE 3 (A) Room-temperature XRD patterns and (B) the locally scanned (200) diffraction lines of NN-BT-xNS ceramics as indicated; (C) the lattice parameters of NN-BT-xNS ceramics as a function of NS content x [Color figure can be viewed at wileyonlinelibrary.com]

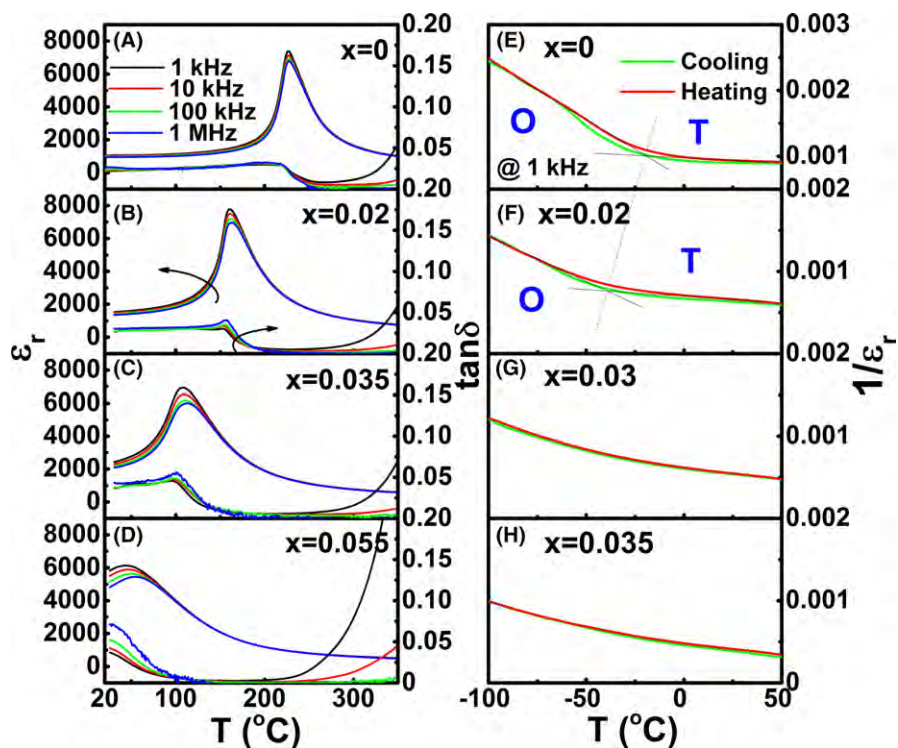
CN=6). The (200) diffraction peaks were fitted by a pseudo-Voigt profile function using the program of MDI Jade, as shown in Figure 3B. The doublet (002)_T/(200)_T

diffraction peak suggested a T symmetry for the 0.9NN-0.1BT ceramic ($x=0$). The splitting of (002)_T and (200)_T lines remained up to $x=0.03$. A single (200) peak appeared as $x>0.04$, indicating an R symmetry. In the composition range of $0.03 \leq x \leq 0.04$, T and R phases were found to coexist, meaning the formation of an MPB between R and T phases. The lattice parameters were calculated as a function of NS content, as shown in Figure 3C. The unit cell volume slightly decreased with increasing the NS content, probably because the radius of Sb⁵⁺ is a bit smaller than that of Nb⁵⁺. Moreover, the tetragonality (c/a) declined with increasing x mainly owing to a drastic decrease in the lattice constant c_T .

3.2 | Dielectric relaxation behavior

Figure 4A-D shows the temperature dependence of the dielectric constant (ϵ_r) and loss tangent ($\tan\delta$) measured at various frequencies for NN-BT-xNS ceramics. The temperature at the dielectric maxima (T_m) rapidly decreased with increasing x . Moreover, the dielectric peak became more and more diffuse and more frequency dependent, indicating a normal to relaxor ferroelectric phase transition with increasing x . This can be more clearly seen from the following measurement of ferroelectric properties. As reported, the 0.9NN-0.1BT ceramic ($x=0$) should be located close to the O-T polymorphic phase boundary, indicating that there should be an O-T polymorphic phase transition near RT.^{29,30} In order to clearly identify this dielectric anomaly, the dielectric constant at 1 kHz was measured

FIGURE 4 Dielectric constant and loss tangent at various frequencies as a function of temperature for unpoled NN-BT-xNS samples with (A) $x=0$, (B) $x=0.02$, (C) $x=0.035$, and (D) $x=0.055$; the inverse of the dielectric constant value versus temperature ($1/\epsilon_r$ vs. T) curves at 1 kHz recorded during heating and cooling for samples with (E) $x=0$, (F) $x=0.02$, (G) $x=0.03$, and (H) $x=0.035$ [Color figure can be viewed at wileyonlinelibrary.com]



during heating and cooling, as shown in Figure 4E-H. An obvious thermal hysteresis around the O-T phase transition temperature (T_{O-T}) was observed for the $x \leq 0.02$ samples. The T_{O-T} value could be estimated by using the intersection point of two tangent lines for the $1/\epsilon_r$ - T curves during heating.³⁵ It can be seen that T_{O-T} was gradually shifted below RT with increasing the NS content x . It seems that the substitution of NS for NN played a role in stabilizing the T phase in a certain composition range, although the tetragonality tended to decline.

3.3 | Polarization switching and electrostrains

Figure 5A indicates P - E hysteresis loops of NN-BT- x NS ceramics. Square well-saturated P - E loops were observed for the $x \leq 0.02$ samples, indicating a normal ferroelectric behavior. With increasing the NS content, P - E loops became slimmer and slimmer, as indicated by a monotonous decrease in the maximum polarization P_{max} , remanent polarization P_r , and coercive field E_c . The values of P_r and E_c were $17 \mu\text{C}/\text{cm}^2$ and $1 \text{ kV}/\text{mm}$, respectively, for the $x=0.035$ composition. The P_r value of the $x=0.055$ sample was nearly zero. This process well corresponded to the formation of dielectric relaxation behavior as mentioned above, meaning a gradual decrease in the domain size. Owing to large random fields from the compositional disorder, the long-range ordered ferroelectric macrodomains would be disrupted into polar nanoregions, which were considered as typical features of a relaxor ferroelectric.^{36,37} These changes were also reflected by bipolar S - E curves as shown in Figure 5B. A gradual change was found from a typical butterfly-shaped S - E curve to a sprout-shaped one. The negative strain S_{neg} drastically dropped with increasing the NS content x , indicating that the amount of irreversible non- 180° domain switching decreased. As $x=0.055$, the S_{neg} value became nearly zero, demonstrating the formation of a pure ergodic relaxor state at RT. At the same time, the positive strain S_{pos} reached the maximum value because of an electric field-induced reversible phase transition from an ergodic relaxor state to a long-range ferroelectric ordering state.³⁷

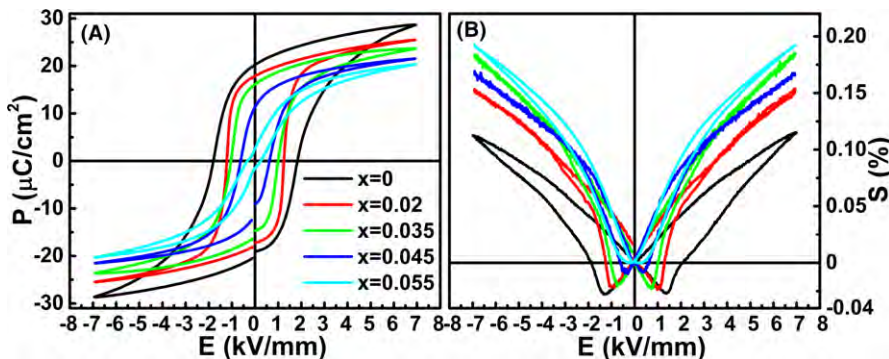


FIGURE 5 (A) P - E hysteresis loops and (B) bipolar S - E curves at 10 Hz for different NN-BT- x NS ceramics as indicated [Color figure can be viewed at [wileyonlinelibrary.com](#)]

3.4 | Phase diagram

According to the analysis of crystal structures and the measurement of dielectric and ferroelectric properties, a composition-temperature phase diagram of the NN-BT- x NS ternary system was plotted, as shown in Figure 6. Above T_m should be the cubic paraelectric phase (C_{PE}) for normal ferroelectrics or a pseudo-cubic ergodic relaxor phase (PC_{ER}) for relaxor ferroelectrics. Below T_m , the phase diagram was segmented into several main phase zones such as O ferroelectric phase (O_{FE}), T ferroelectric phase (T_{FE}), T and R mixed ferroelectric phases ($T_{FE}+R_{FE}$), and R ferroelectric phase (R_{FE}). It can be seen that the high-temperature T phase was stabilized due to the addition of NS, so that low-temperature O phase did not participate into the formation of R and T phase boundary. The kind of phase boundary should differ from that observed in conventional NKN-based ceramics. The latter generally evolved from the high-temperature or low-temperature polymorphic phase transition.^{1,4,6,7} Therefore, the R - T phase boundary

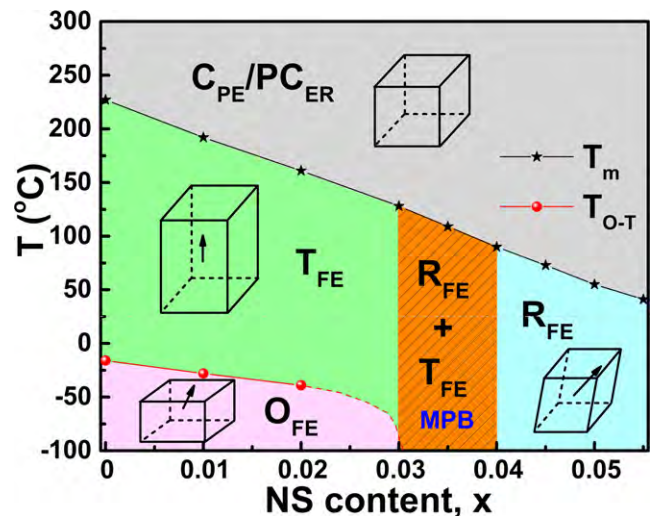


FIGURE 6 Temperature-composition phase diagram of NN-BT- x NS ceramics according to the measurements of dielectric constant, polarization, and strains [Color figure can be viewed at [wileyonlinelibrary.com](#)]

observed in this work should be an MPB as found in PZT or PMN-PT systems. The same type of phase boundary was found in NN-BT-CZ ternary system where it proved to be compositionally driven and temperature insensitive.³⁰

3.5 | Piezoelectric properties and domain morphology

Figure 7 shows RT d_{33} , k_p , Q_m , and $\epsilon_{33}^T/\epsilon_0$ of poled NN-BT- x NS ceramics. It can be found that the electrical properties exhibited obviously compositional dependence. The values of d_{33} and k_p firstly started to increase with x , and then reached their maximum values ($d_{33}=252$ pC/N and $k_p=36\%$) approximately at $x=0.035$, and finally dropped down with further increasing x . The enhancement of piezoelectric and electromechanical properties near $x=0.035$ should be ascribed to the role of the MPB, which would make the polarization switching easier under a poling field by reducing the energy barrier. Both values nearly disappeared with the addition of more NS, mainly owing to the weakening of ferroelectricity. By contrast, the $\epsilon_{33}^T/\epsilon_0$ value increased monotonously because of the enhancement of the relaxation characteristics and the lowering of T_m values. An important feature of NN-based piezoelectric ceramics for resonators/filters applications is the relatively high Q_m .³⁸ The 0.9NN-0.1BT binary ceramics displayed a large Q_m value of ~ 196 , which decreased monotonously with increasing the NS content. A large Q_m of ~ 168 was obtained in the MPB composition of $x=0.035$. Similar to

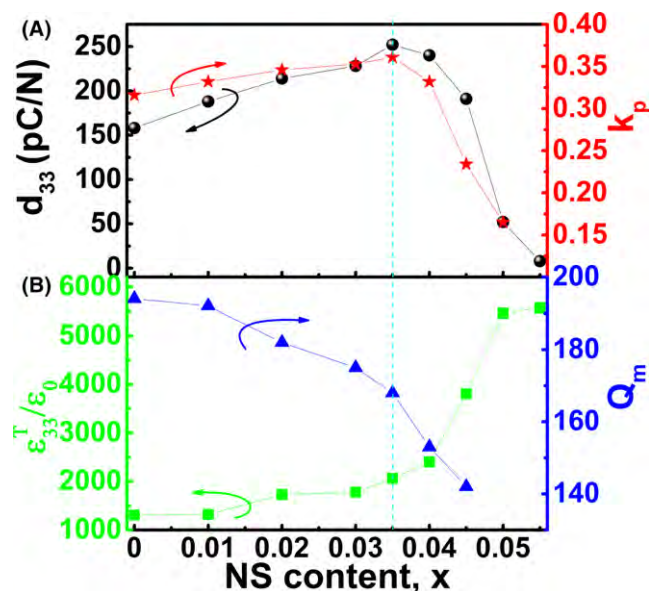


FIGURE 7 (A) Quasi-static piezoelectric coefficient d_{33} and planar electromechanical coupling factor k_p , and (B) dielectric constant $\epsilon_{33}^T/\epsilon_0$ and mechanical quality factor Q_m of poled NN-BT- x NS ceramics as a function of NS content x [Color figure can be viewed at wileyonlinelibrary.com]

the change in E_c , the decrease in Q_m should be attributed to the ease of the domain wall motion accompanied by the enhancement of the dielectric relaxation behavior.

Figure 8 shows the bright-field domain morphology of the $x=0.035$ and $x=0.055$ samples. A typical core-shell structure can be observed within one grain (Figure 8A), in which lamellar domains were in the center and nanodomains with faint contrasts were in the outer shell. These two kinds of domain morphologies should come from T and R phases, respectively. The R -phase compositions exhibited an obvious dielectric relaxation feature, particularly for the $x=0.055$ composition with a typical ergodic relaxor state at RT. The nanodomain morphology (or polar nanoregions) of the R phase could be further confirmed by the dirty-like contrast in the $x=0.055$ sample, as shown in Figure 8B. The coexistence of R and T phases within one grain as well as the existence of nanodomains would be responsible for enhanced piezoelectric responses for the MPB composition ($x=0.035$). The lower domain wall energy of nanodomains would further facilitate the domain switching in response to the external electric field.

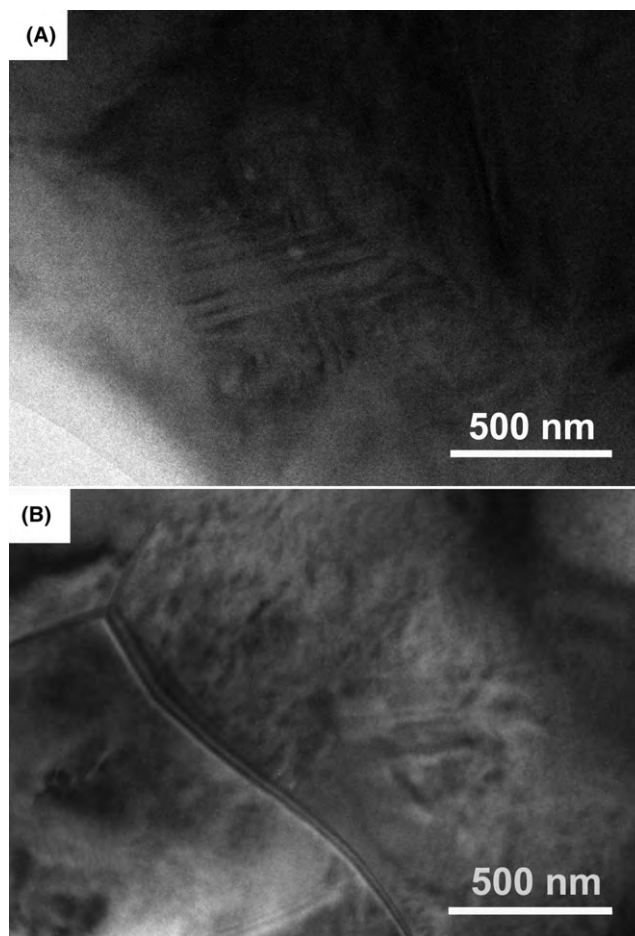


FIGURE 8 Bright-field domain morphology of NN-BT- x NS ceramics with (A) $x=0.035$ and (B) $x=0.055$

3.6 | Temperature dependence of piezoelectric properties

For practical applications, the reliability of piezoelectric devices should be very important. This requires piezoelectric materials to not only have high electrical properties but also an excellent stability such as temperature insensitivity. Figure 9 shows a comparison of temperature-dependent d_{33} , $\tau/d_{33,RT}$ and $k_{p,T}/k_{p,RT}$ values for several representative lead-free ceramics with advanced piezoelectric properties.^{14,20,39–41} It can be seen that the d_{33} and k_p values for the $x=0.035$ composition in current work showed little variation when the annealing temperature (T_a) was lower than T_m , and dropped rapidly when T_a was close to T_m because of gradual disappearance of the ferroelectricity above T_m . Excellent piezoelectric properties of $d_{33}=252$ pC/N and $k_p=36\%$ could keep stable till 100°C during annealing. The excellent temperature stability of piezoelectric properties in the $x=0.035$ composition should be ascribed to the temperature stability of the phase structure owing to the MPB in nature.³⁰ Compared with CZ-substituted NN-BT lead-free materials,³⁰ the

NS-substituted NN-BT ($x=0.035$) exhibited relatively large piezoelectric properties but slightly low T_c , which should mainly be ascribed to higher electronegativity of Sb^{5+} .^{1,19} It is worthy of note that the relative variation of d_{33} and k_p of the $x=0.035$ ceramic in the investigated temperature range was much smaller than that of other lead-free phase-boundary compositions. Modified BT- and NKN-based ceramics exhibited temperature-sensitive piezoelectric properties particularly for phase-boundary compositions owing to the occurrence of the polymorphic phase transition with changing temperature, although their optimized d_{33} could be even higher than 500 pC/N. Although an R-T MPB was achieved in BNT-based lead-free ceramics,^{5,10,14,15} which is responsible for the good temperature stability of piezoelectric properties, yet they still exhibited obvious drawbacks such as the low depolarization temperature ($T_d\sim 70\text{--}100^\circ\text{C}$), the high E_c value ($\sim 3\text{--}4$ kV/mm), and the poor piezoelectric response ($\sim 160\text{--}220$ pC/N). Although excellent thermal stability was found in some nonperovskite ceramics with ultrahigh T_c ,^{42,43} yet perovskite ceramics exhibited an obvious advantage in d_{33} values. A vertical MPB should be basically responsible for the thermally stable piezoelectric and electromechanical properties of the $x=0.035$ composition in an acceptable temperature range, demonstrating good application potentials in future piezoelectric devices.

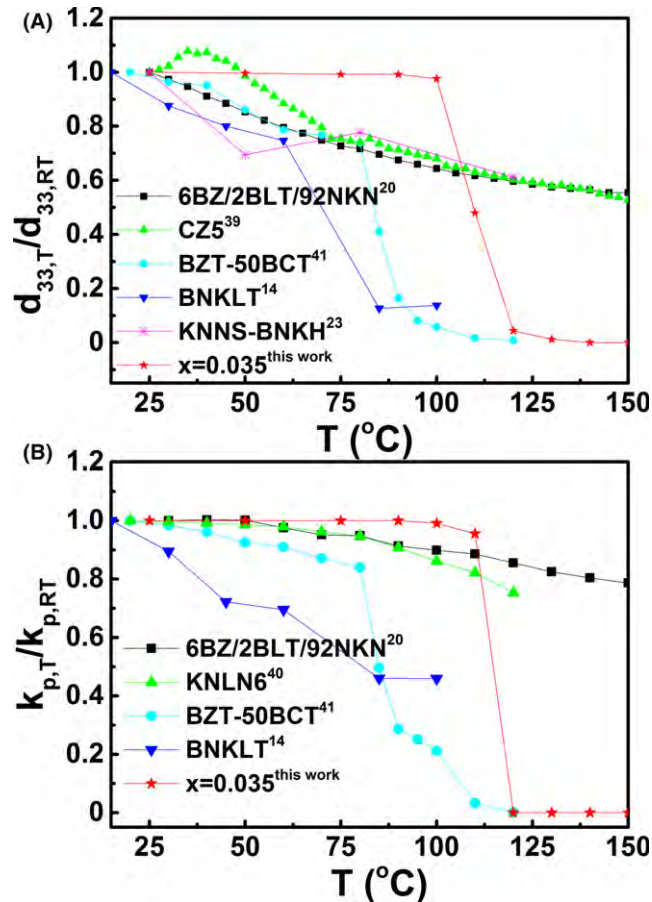


FIGURE 9 A comparison of the temperature dependence of both d_{33} and k_p values relative to their RT values for a few typical materials including the composition in this work and ones reported in the literatures [Color figure can be viewed at wileyonlinelibrary.com]

4 | CONCLUSIONS

A ternary lead-free piezoelectric ceramic based on NN-BT-NS solid solutions was investigated in terms of its microstructure, crystal structure, domain morphology, ferroelectric, and piezoelectric properties. The substitution of NS for NN induced an obvious change in grain morphology from cube-like to sphere-like ones and also an evolution from normal to relaxor ferroelectric phases. Optimum dielectric, piezoelectric, and electromechanical properties of $d_{33}=252$ pC/N, $k_p=36\%$, $Q_m=168$, $\epsilon_{33}^T/\epsilon_0=2063$, and $T_c=109^\circ\text{C}$ were obtained in the composition of $x=0.035$, which was located within a vertical MPB between R and T ferroelectric phases. Compared with other representative lead-free material systems, insufficiency in piezoelectric activities of NN-based lead-free systems was well offset by excellent temperature stability of small-signal piezoelectric properties, showing good application potentials in actuator and sensor devices.

ACKNOWLEDGMENTS

This work was supported by the joint fund of National Natural Science Fund Committee and Large Devices of Chinese Academy of Science (U1432113) and the National Natural Science Foundation of China (51332002).

REFERENCES

1. Saito Y, Takao H, Tani T, et al. Lead-free piezoceramics. *Nature*. 2004;432:84-87.
2. Li JF, Wang K, Zhu FY, Cheng LQ, Yao FZ. (K, Na)NbO₃-based lead-free piezoceramics: Fundamental aspects, processing technologies, and remaining challenges. *J Am Ceram Soc*. 2013;96:3677-3696.
3. Rödel J, Jo W, Seifert KTP, Anton EM, Granzow T, Damjanovic D. Perspective on the development of lead-free piezoceramics. *J Am Ceram Soc*. 2009;92:1153-1177.
4. Wu JG, Xiao DQ, Zhu JG. Potassium-sodium niobate lead-free piezoelectric materials: Past, present, and future of phase boundaries. *Chem Rev*. 2015;115:2559-2595.
5. Shrout TR, Zhang SJ. Lead-free piezoelectric ceramics: Alternatives for PZT? *J Electroceram*. 2007;19:111-124.
6. Zuo RZ, Fu J, Lv DY. Phase transformation and tunable piezoelectric properties of lead-free (Na_{0.52}K_{0.48-x}Li_x)(Nb_{1-x-y}Sb_yTa_x)O₃ system. *J Am Ceram Soc*. 2009;92:283-285.
7. Zuo RZ, Fu J. Rhombohedral-tetragonal phase coexistence and piezoelectric properties of (NaK)(NbSb)O₃-LiTaO₃-BaZrO₃ lead-free ceramics. *J Am Ceram Soc*. 2011;94:1467-1470.
8. Liu WF, Ren XB. Large piezoelectric effect in Pb-free ceramics. *Phys Rev Lett*. 2009;103:257602.
9. Acosta M, Khakpash N, Someya T, et al. Origin of the large piezoelectric activity in (1-x)Ba(Zr_{0.2}Ti_{0.8})O₃-x(Ba_{0.7}Ca_{0.3})TiO₃ ceramics. *Phys Rev B*. 2015;91:104108.
10. Ma C, Guo HZ, Beckman SP, Tan XL. Creation and destruction of morphotropic phase boundaries through electrical poling: A case study of lead-free (Bi_{1/2}Na_{1/2})TiO₃-BaTiO₃ piezoelectrics. *Phys Rev Lett*. 2012;109:107602.
11. Xu K, Li J, Lv X, et al. Superior piezoelectric properties in potassium-sodium niobate lead-free ceramics. *Adv Mater*. 2016;28:8519-8523.
12. Acosta M, Novak N, Jo W, Rödel J. Relationship between electromechanical properties and phase diagram in the Ba(Zr_{0.2}Ti_{0.8})O₃-x(Ba_{0.7}Ca_{0.3})TiO₃ lead-free piezoceramic. *Acta Mater*. 2014;80:48-55.
13. Takenaka T, Maruyama KI, Sakata K. (Bi_{1/2}Na_{1/2})TiO₃-BaTiO₃ system for lead-free piezoelectric ceramics. *Jpn J Appl Phys*. 1991;30:2236-2239.
14. Zhang BY, Wu JG, Wu B, Xiao DQ, Zhu JG. Effects of sintering temperature and poling conditions on the electrical properties of Bi_{0.5}(Na_{0.70}K_{0.20}Li_{0.10})_{0.50}Ti_{0.50}O₃ piezoelectric ceramics. *J Alloy Compd* 2012;525:53-57.
15. Rao BN, Senyshyn A, Olivi L, Sathe V, Ranjan R. Maintaining local displacive disorders in Na_{0.5}Bi_{0.5}TiO₃ piezoceramics by K_{0.5}Bi_{0.5}TiO₃ substitution. *J Eur Ceram Soc*. 2016;36:1961-1972.
16. Damjanovic D. A morphotropic phase boundary system based on polarization rotation and polarization extension. *Appl Phys Lett*. 2010;97:062906.
17. Ma C, Tan X, Dul'kin E, Roth M.. Domain structure-dielectric property relationship in lead-free (1-x)(Bi_{1/2}Na_{1/2})TiO₃-xBaTiO₃ ceramics. *J Appl Phys*. 2010;108:104105.
18. Dai YJ, Zhang XW, Zhou GY. Phase transitional behavior in K_{0.5}Na_{0.5}NbO₃-LiTaO₃ ceramics. *Appl Phys Lett*. 2007;90:262903.
19. Zuo RZ, Fu J, Lv DY, Liu Y. Antimony tuned rhombohedral-orthorhombic phase transition and enhanced piezoelectric properties in sodium potassium niobate. *J Am Ceram Soc*. 2010;93:2783-2787.
20. Wang RP, Wang K, Yao FZ, et al. Temperature stability of lead-free niobate piezoceramics with engineered morphotropic phase boundary. *J Am Ceram Soc*. 2015;98:2177-2182.
21. Yao FZ, Wang K, Jo W, et al. Diffused phase transition boosts thermal stability of high-performance lead-free piezoelectrics. *Adv Funct Mater*. 2016;26:1217-1224.
22. Zuo RZ, Qi H, Fu J. Strain effects of temperature and electric field induced phase instability in (Na, K)(Nb, Sb)O₃-LiTaO₃ lead-free ceramics. *J Eur Ceram Soc*. 2017;37:2309-2313.
23. Zheng T, Wu HJ, Yuan Y, et al. The structural origin of enhanced piezoelectric performance and stability in lead free ceramics. *Energy Environ Sci*. 2017;10:528-537.
24. Zhang MH, Wang K, Du YJ, et al. High and temperature-insensitive piezoelectric strain in alkali niobate lead-free perovskite. *J Am Chem Soc*. 2017;139:3889-3895.
25. Acker J, Kungl H, Schierholz R, Wagner S, Eichel RA, Hoffmann MJ. Microstructure of sodium-potassium niobate ceramics sintered under high alkaline vapor pressure atmosphere. *J Eur Ceram Soc*. 2014;34:4213-4221.
26. Acker J, Kungl H, Hoffmann MJ. Sintering and microstructure of potassium niobate ceramics with stoichiometric composition and with potassium- or niobium excess. *J Eur Ceram Soc*. 2013;33:2127-2139.
27. Juang YD, Dai SB, Wang YC, et al. Phase transition of Li_xNa_{1-x}NbO₃ studied by Raman scattering method. *Solid State Commun*. 1999;111:723-728.
28. Lin DM, Kwok KW. Ferroelectric and piezoelectric properties of new NaNbO₃-Bi_{0.5}K_{0.5}TiO₃ lead-free ceramics. *J Mater Sci: Mater Electron*. 2010;21:1060-1065.
29. Zeng JT, Kwok KW, Chan HLW. Ferroelectric and piezoelectric properties of Na_{1-x}Ba_xNb_{1-x}Ti_xO₃ ceramics. *J Am Ceram Soc*. 2006;89:2828-2832.
30. Zuo RZ, Qi H, Fu J. Morphotropic NaNbO₃-BaTiO₃-CaZrO₃ lead-free ceramics with temperature-insensitive piezoelectric properties. *Appl Phys Lett*. 2016;109:022902.
31. Chan IH, Sun CT, Hough MP, Chu SY. Sb doping effects on the piezoelectric and ferroelectric characteristics of lead-free Na_{0.5}K_{0.5}Nb_{1-x}Sb_xO₃ piezoelectric ceramics. *Ceram Int*. 2011;37:2061-2068.
32. Cho GC, Dodds J, Santamarina JC. Particle shape effects on packing density, stiffness, and strength: Natural and crushed sands. *J Geotech Geoenviron Eng*. 2006;132:591-602.
33. Svoboda J, Riedel H, Zipse H. Equilibrium pore surfaces, sintering stresses and constitutive equations for the intermediate and late stages of sintering—I. computation of equilibrium surfaces. *Acta Metall Mater* 1994;42:435-443.
34. Qin RS, Fan Z. Fractal theory study on morphological dependence of viscosity of semisolid slurries. *Mater Sci Technol*. 2001;17:1149-1152.
35. Mitsui T, Tatsuzaki I, Nakamura E. An Introduction to the Physics of Ferroelectrics. New York: Gordon Breach Sci. Pub.; 1976; 443 pp.
36. Bokov AA, Ye ZG. Recent progress in relaxor ferroelectrics with perovskite structure. *J Mater Sci*. 2006;41:31-52.
37. Jo W, Dittmer R, Acosta M, et al. Giant electric-field-induced strains in lead-free ceramics for actuator applications-status and perspective. *J Electroceram*. 2012;29:71-93.

38. Mitra S, Kulkarni AR. Synthesis and electrical properties of new lead-free $(100-x)(\text{Li}_{0.12}\text{Na}_{0.88})\text{NbO}_3-x\text{BaTiO}_3$ ($0 \leq x \leq 40$) piezoelectric ceramics. *J Am Ceram Soc.* 2016;99:888-895.
39. Wang K, Yao FZ, Jo W, et al. Temperature-insensitive (K, Na) NbO_3 -based lead-free piezoactuator ceramics. *Adv Funct Mater.* 2013;23:4079-4086.
40. Hao JG, Xu ZJ, Chu RQ, et al. Enhanced temperature stability of modified $(\text{K}_{0.5}\text{Na}_{0.5})_{0.94}\text{Li}_{0.06}\text{NbO}_3$ lead-free piezoelectric ceramics. *J Mater Sci.* 2009;44:6162-6166.
41. Lu SB, Xu ZK, Su S, Zuo RZ. Temperature driven nano-domain evolution in lead-free $\text{Ba}(\text{Zr}_{0.2}\text{Ti}_{0.8})\text{O}_3-50(\text{Ba}_{0.7}\text{Ca}_{0.3})\text{TiO}_3$ piezoceramics. *Appl Phys Lett.* 2014;105:032903.
42. Cai K, Jiang F, Deng PY, Ma JT, Guo D. Enhanced ferroelectric phase stability and high temperature piezoelectricity in PN ceramics via multisite co-doping. *J Am Ceram Soc.* 2015;98:3165-3172.
43. Cai K, Huang CC, Guo D. Significantly enhanced piezoelectricity in low-temperature sintered Aurivillius-type ceramics with ultra-high Curie temperature of 800 & #xB0;C. *J Phys D: Appl Phys.* 2017;50:155302.

How to cite this article: Qi H, Zhang H, Zuo R. NaNbO_3 - BaTiO_3 - NaSbO_3 lead and potassium-free ceramics with thermally stable small-signal piezoelectric properties. *J Am Ceram Soc.* 2017; 100:3990–3998. <https://doi.org/10.1111/jace.14944>